

Electronic Supplementary Information (ESI)†  
for

**Atomistic determination of the surface structure of Cu<sub>2</sub>O (111): experiment and theory**

Rui Zhang,<sup>‡</sup> Liang Li,<sup>‡</sup> Laszlo Frazer,<sup>‡</sup> Kelvin B. Chang,<sup>‡</sup> Kenneth R. Poeppelmeier,<sup>‡,d</sup> Maria K. Y. Chan,<sup>‡</sup>  
and Jeffrey R. Guest<sup>\*a</sup>

<sup>a</sup> Center for Nanoscale Materials, Argonne National Laboratory, 9700 South Cass Avenue, Argonne, IL 60439, USA.

<sup>b</sup> Centre of Excellence in Exciton Science, UNSW, Sydney, NSW 2052 Australia and Monash University, Clayton, Victoria, 3800 Australia

<sup>c</sup> Department of Chemistry, Northwestern University, 2145 Sheridan Road, Evanston, IL 60208, USA

<sup>d</sup> Chemical Sciences and Engineering Division, Argonne National Laboratory, 9700 South Cass Avenue, Argonne, IL 60439, USA

<sup>‡</sup>These authors contributed equally to this work.

Corresponding author: [jrguest@anl.gov](mailto:jrguest@anl.gov)

## S1: Simulated STM images of (111) surface without $\text{Cu}_v$ ions

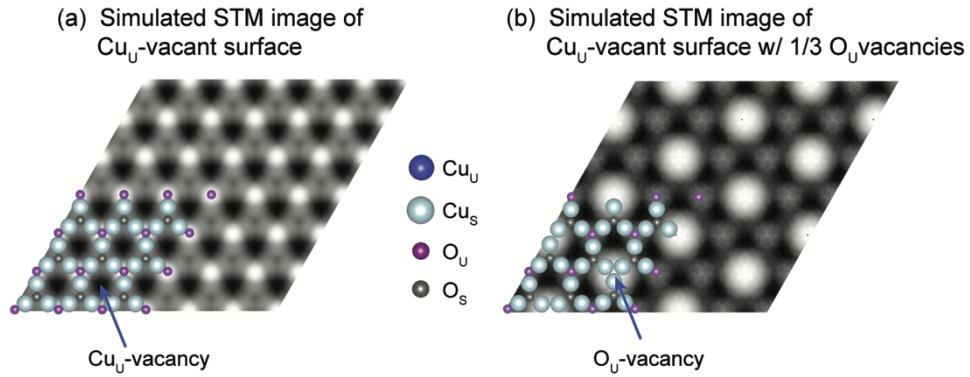


**Figure S1.** Atomic structure and corresponding simulated STM image of the (111) surface without surface  $\text{Cu}_v$  ions ( $\text{Cu}_v$ -vacant surface, see in main text). (a) Simulated STM image (+1.5 V) with the relaxed atomic structure overlaid on top of the image. (b) Simulated STM image (+1.5 V) of the  $\text{Cu}_v$ -vacant surface with removal of  $1/3 \text{O}_v$  ions. After removing a  $\text{O}_v$  ion the three saturated copper ions ( $\text{Cu}_s$ ) combine together, forming a larger and much bright dot feature on the image, which is, however, not seen in our experimental STM images. Moreover, the inter-atomic spacing between the three combined  $\text{Cu}_s$  ions is much smaller than the value of  $4.65 \text{ \AA}$  measured from bright triangular defect in Fig. 3a.

## S2: Models of Cu<sub>2</sub>O(111) surface structures

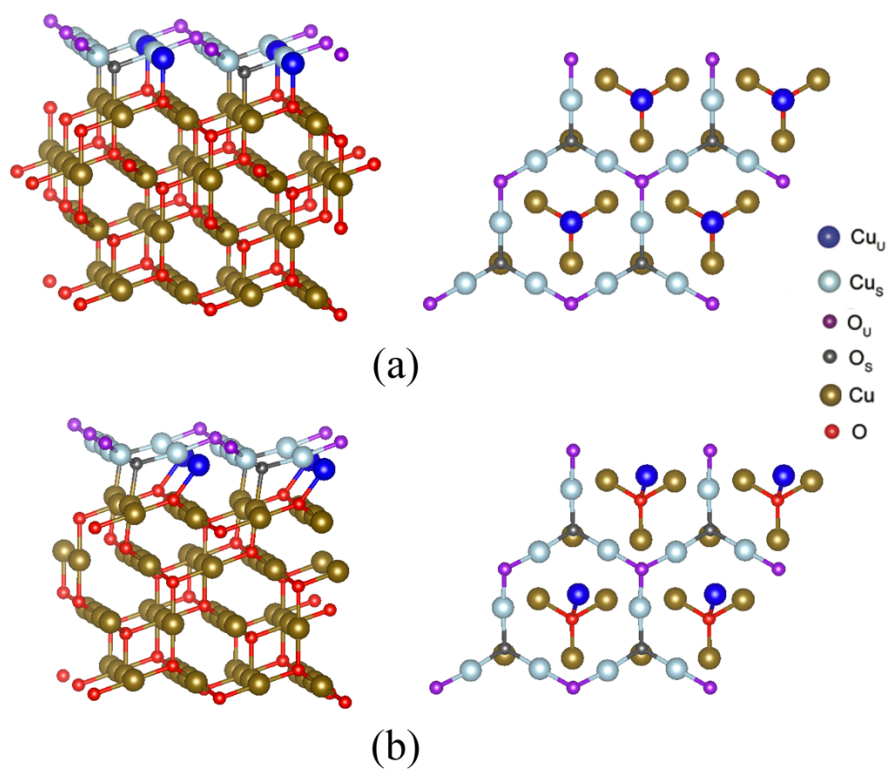


**Figure S2.** Side (left) and top (right) views of (a) unrelaxed and (b) DFT-relaxed Cu<sub>2</sub>O (111) surface structures. After structural relaxation, the height of Cu<sub>u</sub> atoms is lower than that of Cu<sub>s</sub> atoms, and Cu<sub>u</sub> atoms are not at the centers of the hexagons formed by surface Cu<sub>s</sub>.

### S3: Simulated STM images of (111) surface with isolated $O_v$ -vacancy

Fig. S3 shows the simulated STM images of a  $3\times 3$   $\text{Cu}_2\text{O}$  (111) surface with one oxygen vacancy. From the relaxed structure, it is obvious that three  $\text{Cu}_v$  atoms surrounding the oxygen vacancy were displaced toward the oxygen vacancy after structural relaxation. Under +1.5 V simulation voltage (Fig. S3a), the simulated image shows similar features as the surface with a higher oxygen vacancy concentration (Fig. 3e), and also closely resembles the experimental STM image (Fig. 3a). Under -1.5 V bias voltage (Fig. S3b), the oxygen vacancy site appears as a large protrusion, which is also consistent with experiment (Fig. 1d).

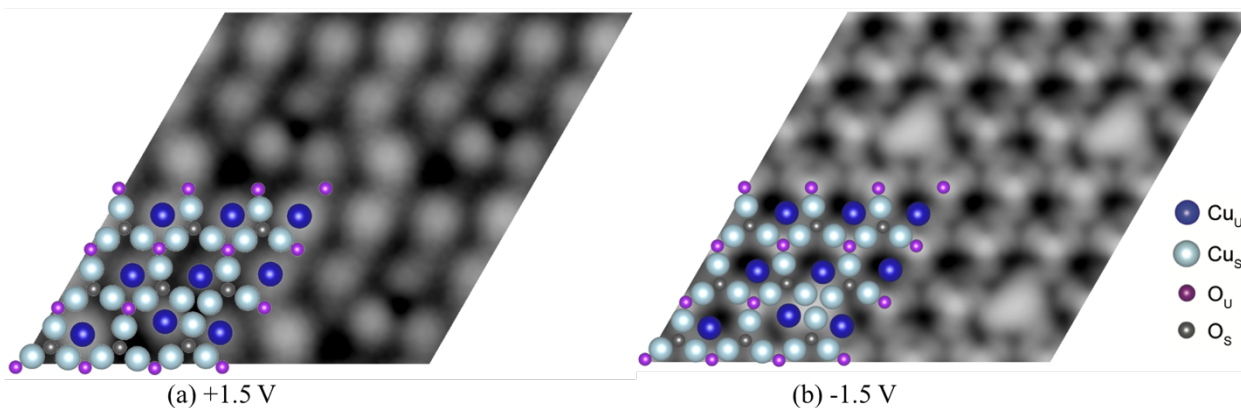


**Fig. S3.** Atomic structures and simulated STM images of  $3\times 3$   $\text{Cu}_2\text{O}$  (111) surface with one oxygen vacancy under bias voltages of (a) +1.5 V and (b) -1.5 V.

#### S4: Defect formation energies on the Cu<sub>2</sub>O (111) surface

The formation energies of Cu and O vacancies are defined as

$$E_{form} = \left( E_{surf}^{vac} + \sum_{i=Cu,O} n_i \mu_i \right) - E_{surf}^{clean}$$

where  $E_{surf}^{vac}$  and  $E_{surf}^{clean}$  indicate the energies of defected and clean surfaces, respectively.  $n_i$  ( $i$  indicates Cu or O) is the number of missing surface Cu or O atoms, and  $\mu_i$  represents the chemical potential of the missing atoms, which are correlated by  $2\mu_{Cu} + \mu_O = \mu_{Cu_2O}^{bulk}$ . Under oxygen-poor condition,  $\mu_{Cu}$  and  $\mu_{Cu_2O}^{bulk}$  are taken as the DFT energies of bulk Cu and Cu<sub>2</sub>O, respectively, and  $\mu_O$  is computed accordingly. The mixing of GGA and GGA+U energies was taken into account following the formulism proposed by Jain *et al.*<sup>1</sup>

The vacancy formation energies were calculated using a 2×2 Cu<sub>2</sub>O (111) surface model. Fig. S4 presents the relaxed geometries and formation energies of Cu<sub>2</sub>O (111) surface with various types of surface vacancies. Based on the DFT calculation, Cu vacancy is the energetically favorable defect type, with the formation energy being negative (Figs. S4b and c), while O vacancy results in highly positive formation energies (Figs. S4e and f), indicating that it is not thermodynamically stable.

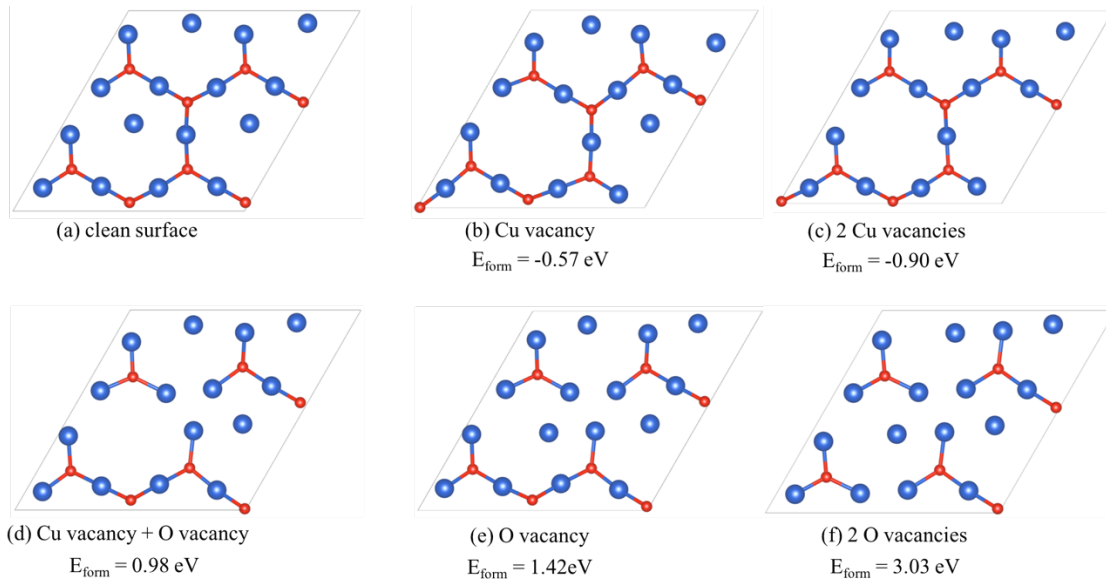


**Fig. S4.** (a) Geometry of clean 2×2 Cu<sub>2</sub>O (111) surface. DFT-calculated geometries and formation energies of defected Cu<sub>2</sub>O (111) surface with (b) single Cu vacancy, (c) single O vacancy, (d) double Cu vacancies, (e) one Cu and one O vacancy and (f) double oxygen vacancies. Blues and red spheres represent the surface Cu and O atoms, respectively.

## S5: Autocorrelation of STM images of Cu<sub>2</sub>O (111)

In order to develop a quantitative understanding of the likelihood of O defects grouping together, we performed an autocorrelation on the images. At  $V=-1.5$  V (Fig. 1d), O vacancies are identified by distinct protrusions (Fig. 1d); therefore, a simple binary threshold filter which bins the points as one or zero based on height creates a binary map of the defects. After subtracting a plane from the data and performing three nearest pixel averages, we performed this filter to generate a binary map of the defects as seen in Fig. S5, left; topographic values  $>1.3$  Å above the pristine surface were converted to 1's, below were converted to 0's to produce  $T(x_i, y_j)$ . Then we performed a simple autocorrelation:

$$AC(\Delta x, \Delta y) = \sum_{i=0}^N \sum_{j=0}^N [T(x_i, y_j) \times T(x_i - \Delta x, y_j - \Delta y)]$$

In Fig. S5, middle, we show the autocorrelation function on the same length scale as the original binary image. A zoom in is shown in Fig. S5, right. The self-correlation peak appears in the center. The periodicity of the Cu<sub>2</sub>O (111) unit cell is apparent in the image. Additionally, there are clearly missing peaks in the autocorrelation at the nearest neighbor sites and the next nearest neighbor sites along the primary axes, indicating that these defects are unlikely to be found at these relative locations (marked in yellow circles). In other words, these defects are more likely to be found occupy sites that are further apart than nearby one another occupying nearest neighbor or next-nearest neighbor sites (along primary axes).

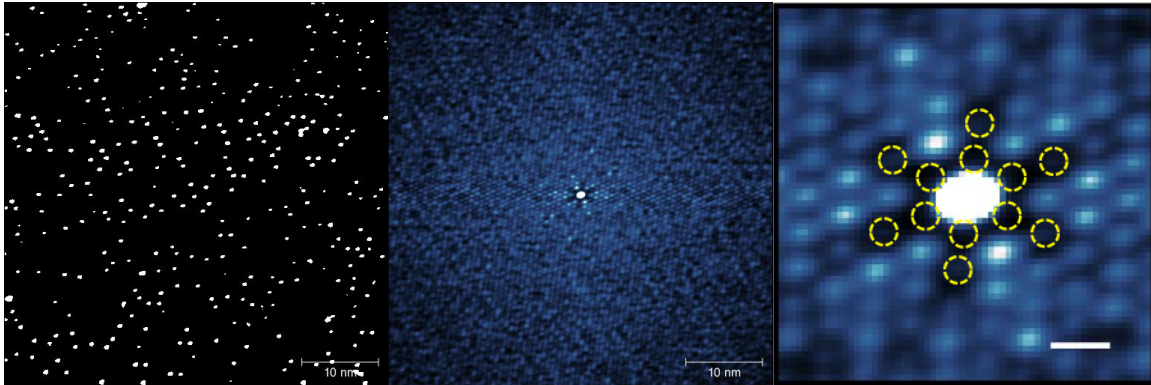


**Fig. S5.** Autocorrelation function. Left: Binary image  $T(x_i, y_j)$  after performing the threshold process (same data as Fig. 1d). The autocorrelation function  $AC(\Delta x, \Delta y)$  is shown in the middle panel and zoomed in in the right panel, where dips in the map are shown with yellow circles (scale bar 1 nm).

**References:**

- 1 A. Jain, G. Hautier, S. P. Ong, C. J. Moore, C. C. Fischer, K. a. Persson and G. Ceder, *Phys. Rev. B*, 2011, **84**, 045115.